Aerodynamic analysis of toroidal propellers in forward flight

Oliviu SUGAR-GABOR*,[1], Usman ALI[1], Amir NOURIAN[1]

*Corresponding author
[1]Fluids and Aerodynamics Research Group (FLAIR),
School of Science, Engineering and Environment, University of Salford,
42 The Crescent, Salford, M5 4WT, United Kingdom,
o.sugar-gabor@salford.ac.uk*

DOI: 10.13111/2066-8201.2026.18.2.14

Received: 13 April 2026/ Accepted: 26 April 2026/ Published: June 2026

Abstract: *Research is being conducted to develop a new generation of propellers that can enable quieter and more efficient flight. One promising development in this area are Toroidal propellers, for which the blades are shaped as a closed loop. Studies have been conducted for vertical lift, as well as for marine propulsion systems. Fewer studies have focused on the design and performance of Toroidal propellers for advance ratios, airspeeds and Reynolds number values typically encountered during the forward flight of fixed-wing aircraft. The present work uses Computational Fluid Dynamics to assess the aerodynamic performance of Toroidal propellers in operating conditions having low forward flight speeds and high revolutions per minute. Two Toroidal propeller geometries are designed, using blade chord and pitch angle distributions taken from classical Minimum Induced Loss propellers. The aerodynamic analysis of both designs is conducted over a range of advance ratios between 0.40 and 1.25. Aerodynamic results show that, at fixed advance ratio values, the Toroidal propellers can sustain much higher thrust coefficients compared to both Minimum Induced Loss and commercially available propellers, at comparable efficiencies.*

Key Words: *toroidal propeller, propeller analysis, propeller design, computational fluid dynamics, low-Reynolds propellers*

1. INTRODUCTION

The efficiency of propulsion systems remains a significant issue in aerospace and maritime applications, demanding continuous improvements in the design of propellers. Toroidal propellers, characterised by their unique design in which the tips of the blades are connected in a closed loop, have demonstrated outstanding performance with Vertical Take-off and Landing (VTOL) aircraft and hover operations [2-3]. Modern propellers can achieve efficiencies as high as 0.90 [4, 5] but generate considerable aerodynamic noise and there is a trade-off between performance and noise, as it has been observed that propeller designs that have higher efficiency can produce higher noise [6]. Toroidal propellers were originally studied the 1930s and 1940s [7, 8]. It is important to distinguish toroidal propellers from shrouded or ducted rotors [1, 14], which benefit from forces acting on the shroud itself rather than from the closed-loop blade tip geometry. They became used with the introduction of VTOL aircraft, and since then, their capabilities have been investigated and refined by researchers for applications in vertical take-off and hovering in Unmanned Aerial Vehicle

(UAV) systems [9, 22]. The closed-loop geometry of Toroidal propellers offers many design advantages, including the potential for noise reduction, especially at frequencies most relevant to human perception, as suggested by [11, 12], though not investigated in the present work. The vortex shedding in Toroidal propellers is spread along the continuous loop of the blade which mitigates the primary source of noise present in conventional propellers [10-12]. Computational Fluid Dynamics (CFD) simulations have confirmed this hypothesis, showing that the closed-loop design stabilises airflow and decreases blade tip vortices in Toroidal propellers [13]. The early success of Toroidal propellers in VTOL drone technology indicates that they can potentially be used in a wider range of operation of UAV systems [11].

Sebastian and Strem [15] demonstrated how closed loop design in Toroidal propellers can enhance structural integrity and reduce high-pitch noise without sacrificing the propeller efficiency. Vu [11] numerically evaluated the performance of four different Toroidal propeller shapes, focusing on reducing noise levels generated by blade tip vortices. Combey [16] conducted a CFD study on Toroidal Joined Blade Tips (T-JBT) electric VTOL and Urban Air Mobility (UAM) applications, demonstrating a Thrust Coefficient (C_T) increase from 0.149 in F29 to 0.212 in T-JBT, and a Torque Coefficient (C_Q) increase from 0.018 to 0.039. Alm et al. [12] conducted an experimental study to compare conventional and Toroidal propellers in terms of thrust, efficiency and noise. The authors noted that the traditional 2-bladed design produced higher thrust, while the Toroidal design offered noise reduction.

Beyond aerospace, the Toroidal propeller geometry has also attracted significant interest for hydrodynamic applications in marine environments. Xiang and Wang [17] conducted a study on a novel Toroidal propeller design to improve hydrodynamic and noise performance of underwater vehicle propulsion systems by mitigating issues like tip cavitation found in conventional propellers at high speeds. Wang [18] addressed the hydrodynamic performance of a novel Toroidal propeller (T421) and assessed the influence of four geometric design parameters on hydrodynamic thrust, efficiency and pressure distribution.

Toroidal propellers have been effectively studied in several VTOL applications, including multirotor drones and UAV systems. It is important to note that these applications focused on primarily on hovering [19]. For forward flight, researchers have established various performance benchmarks for traditional propeller designs in small-scale propulsion systems operating at low Reynolds numbers [20]. The work conducted by Brandt [21] is significant in this domain. However, the potential benefits of Toroidal propellers under cruising conditions remain largely unexplored to date. This research represents an investigation of Toroidal propellers specifically designed for forward flight conditions in UAV systems. It addresses a recognised gap by investigating the aerodynamic properties and efficiency metrics of Toroidal propellers designed for cruising flight conditions rather than hover and vertical flight. This CFD study aims to establish a performance baseline for toroidal propellers in forward flight and identify key areas for future research and optimisation.

2. METHODOLOGY

2.1 Operating conditions and propeller characteristics

To test the performance of the Toroidal propeller in forward flight, a set of operating conditions characteristic to small Unmanned Aerial Vehicles (UAVs) was selected. More specifically, a range of fixed-wing UAVs with a maximum take-off mass under 7 kg was analysed. These included the JOUAV CW-007 [23], the Sparkle Tech Long Range UAV [24], the Athlon Avia A1-CM Furia [25] and the Penguin C MK2 [26], among others. The various designs have cruising speeds between $17\ m/s$ and $22\ m/s$ and typical propeller diameters of $11-12$ inch ($279-305\ mm$). Most of the UAVs analysed use a brushless electric motor connected to a $LiPo$ (Lithium-Polymer) battery. Considering motors suitable for $11-12$ inch propellers (such as the T-Motor MN3110 [27] or the T-Motor 2216 [28]) and considering an economical throttle setting of $50\%-60\%$, an RPM in the range of $5000-6000$ is typically achieved. This allows to set the target operating conditions for the Toroidal propeller as indicated in Table 1.

Table 1 – Target operating conditions

Parameter	Value
Airspeed	$19\ [m/s]$
Altitude	Sea Level
RPM	5000
Advance Ratio	0.75

The diameter is set to $12\ inch$, and only the case of a 2-bladed propeller is considered in this study. To keep the design of the propeller as consistent as possible, a required thrust value is set based on the requirements of the fixed-wing UAVs mentioned earlier. Considering a vehicle mass of $7\ kg$ (or $68.7\ N$) and an in-flight lift-to-drag ratio of 10, a nominal thrust force of $6.87\ N$ is targeted. The desired propeller characteristics are summarised in Table 2.

Table 2 – Desired classical propeller characteristics

Parameter	Value
Number of Blades	2
Propeller Diameter	$305\ [mm]$
Target Thrust	$6.87\ N$
Hub Radius	$10\ [mm]$
Blade Aerofoil	$Clark\ Y$
Blade Design Lift Coefficient	0.80

2.2 Classical propeller design

The design of the Toroidal propeller is carried out in two stages. In the first stage, the blade chord and pitch angle distributions along the radius are determined with the help of a straight-bladed (classical) propeller that is required to operate under the same conditions (defined in Tables 1 and 2) as the Toroidal propeller. Then, in the second stage, the geometry of these blades is modified to create the closed-loop design characteristic for Toroidal propellers.

The classical propeller design is achieved using the XROTOR code [29]. The blade chord and pitch angle distributions are required to achieve a Minimum Induced Loss (MIL) circulation distribution [30] and are depicted in Figure 1 under the name MIL-1. While ensuring aerodynamic optimality, MIL designs can have very narrow chord distributions towards the hub, leading to high structural stresses. As the present study is focused on aerodynamic performance, the very narrow chord towards the hub does not pose any challenges, and MIL-1 will be fully analysed to serve as a benchmark. Nonetheless, for any future experimental development and testing, a fuller chord distribution towards the hub is advantageous from a practical manufacturing point of view. A parametric study was conducted by varying the target advance ratio by ± 0.10 around the nominal value of 0.75 and monitoring the change in the chord distribution. For a design advance ratio of approximately 0.85, but with the other conditions defined in Tables 1 and 2 remaining constant, the calculated MIL geometry shows a much fuller chord distribution towards the hub region. The new design is named MIL-2 and will also be fully analysed to serve as the second benchmark of the study.

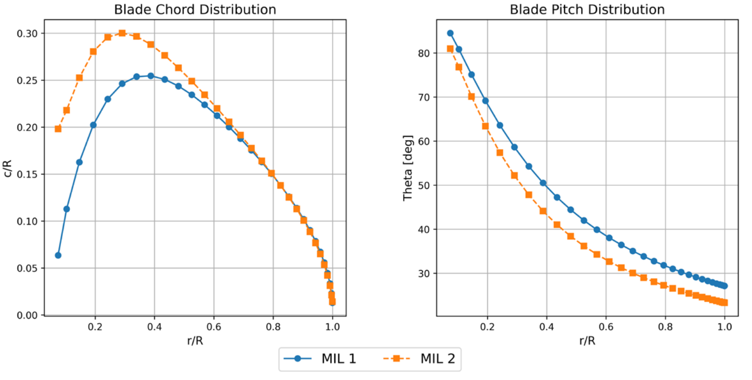

Fig. 1 – Nondimensional chord and blade pitch angle distributions along the nondimensional radial coordinates for the MIL propellers

2.3 Toroidal propeller design

Changing the blade shape from the classical straight blade to the closed-loop shape requires defining a sequence of modifications that, ideally, can be implemented to a wide range of blades. Satisfying this condition of a repeatable approach that can be used regardless of the blade chord and pitch angle distributions is the foundation of the method implemented in this work. It is important to note that the method is not a self-contained design framework, as it cannot provide a complete blade geometry based solely on a set of desired propeller performance characteristics and geometry constraints. The proposed method represents a technique for the modification of an existing blade geometry, that nonetheless provides advantages in terms of performance and opens avenues for the future development of a true design process applicable to Toroidal propellers.

As starting point, the blades of the Toroidal propeller are constructed using the blade chord and pitch angle distributions of the MIL propeller. As two different MIL propellers were generated, two different Toroidal propellers will also be generated: Toroidal-1, using the chord and pitch angle data from MIL-1, and Toroidal-2, using the data from MIL-2. Figure 2 shows three plane views (front, top, and side) of both Toroidal propellers.

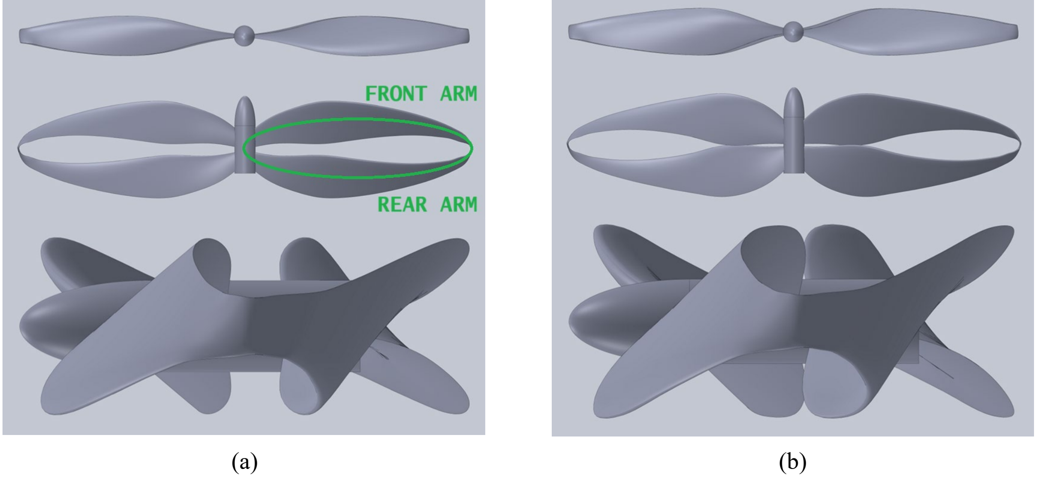

(a) (b)

Fig. 2 – Front, top and side views of (a) Toroidal-1 and (b) Toroidal-2 propellers

Considering a cartesian frame of reference, the propeller disk is in the XZ plane, with the Y axis being the rotation axis. An ellipse is generated in the YZ plane, with the major axis equal to the propeller radius. The minor axis is set equal to 0.25 of the major axis. This value was found by numerical experimentation, being observed that for a minor axis to major axis ratio of 0.25 the resulting Toroidal propeller generates the largest thrust force for the least shaft torque. An illustration of the ellipse is depicted over the top view of Toroidal-1 in Figure 2 (a). The front and rear arms of the ellipse represent guiding curves for constructing the closed-loop blades. A discrete number of radial positions is selected between the radius of the hub and the radius of the propeller. For each radial position, the blade aerofoil is scaled according to the local chord and rotated according to the local pitch angle. Two copies of this aerofoil are then created, the first being positioned such that its quarter-chord point lies on the front arm of the ellipse, and the second positioned such that its quarter-chord point lies on the rear arm.

To ensure a smooth curvature of both front and rear blades, especially towards the tip region, the local aerofoil sections are further adjusted such that each planar surface containing the aerofoil curve is made normal to the corresponding ellipse arm at the quarter-chord point. Joining the front and rear blades at the tip to form a closed loop requires one further adjustment. For blade sections located at radial positions $r/R > 0.95$, the pitch angle is progressively removed such that the last section of both front and rear blades has zero pitch. The closed-loop blade construction process proposed in this work ensures the solidity of the Toroidal propeller remains approximately the same as the solidity of the classical propeller based on which it is constructed. In this context, propeller solidity is referred to as being the ratio between the blade area and the disk area as observed in the XZ (front) plane. The overall blade area (wetted area) is, of course, doubled compared to the classical propeller. While this doubled wetted area is a characteristic shared with 4-blade propellers, the comparison to the 2-blade MIL baseline is intentional, as this study's aim is to isolate the aerodynamic effect of the closed-loop geometric transformation itself.

2.4 Propeller performance coefficients

For clarity, and to make the work relatively self-contained, the definitions of the most common propeller performance coefficients are briefly presented. Let T be the thrust force, Q the shaft torque, P the shaft power, ρ the air density, n the number of revolutions per second and D the propeller diameter. Then, the thrust, torque and power coefficients are given by:

$$C_T = \frac{T}{\rho n^2 D^4} \qquad C_Q = \frac{Q}{\rho n^2 D^5} \qquad C_P = \frac{P}{\rho n^3 D^5} \tag{1}$$

If V is the airspeed, the advance ratio is given by:

$$J = \frac{V}{nD} \tag{2}$$

Lastly, the propeller efficiency is given by:

$$\eta = J\frac{C_T}{C_P} \tag{3}$$

2.5 Numerical model

The aerodynamic performance of the Toroidal propeller is investigated using the ANSYS FLUENT package [31]. The flow is governed by the incompressible Navier-Stokes equations:

$$\nabla \cdot \mathbf{u} = 0$$
$$\frac{\partial \mathbf{u}}{\partial t} + \nabla \cdot (\mathbf{u}\mathbf{u}) = -\nabla p + \nu \Delta \mathbf{u} \tag{4}$$

Here, $\mathbf{u} = (u, v, w)^T$ is the velocity vector, p is the static pressure and ν is the (constant) kinematic viscosity. In the turbulent case, the equations are transformed into the Reynolds-Averaged Navier-Stokes (RANS) equations. In the present work, the eddy viscosity approach is used, in which the eddy viscosity ν_t is added to the laminar viscosity ν and closure of the model is achieved using the $k - \varepsilon$ turbulence model [32]:

$$\frac{\partial k}{\partial t} + \nabla \cdot (\mathbf{u}k) = \nabla \cdot (D_k \nabla k) + G - \varepsilon$$
$$\frac{\partial \varepsilon}{\partial t} + \nabla \cdot (\mathbf{u}\varepsilon) = \nabla \cdot (D_\varepsilon \nabla \varepsilon) + c_1 G \frac{\varepsilon}{k} - c_2 \frac{\varepsilon^2}{k} \tag{5}$$

Here, k is the turbulent kinetic energy and ε is the turbulent dissipation rate. D_k is the effective diffusivity for k and is given by $D_k = \nu + \nu_t/\sigma_k$. Similarly, D_ε is the effective diffusivity for ε and is given by $D_\varepsilon = \nu + \nu_t/\sigma_\varepsilon$. G represents the turbulence generation.

The problem of the rotating propeller (with constant RPM) is treated as a steady-state problem with respect to a moving (non-inertial) reference frame. The equations are solved using a cell-centred finite-volume method using the settings summarised in Table 3.

Table 3 – Numerical solver setup

Feature	Setup
Solver	Pressure Eq.-Based Segregated Solver
Algorithm	SIMPLE [33]
Pressure Eq. Discretisation	2nd Order Centred
Momentum Discretisation	2nd Order Upwind
Turbulence Discretisation	2nd Order Upwind
Gradients	Least Squares
Convergence Acceleration	AMG with Gauss-Seidel Smoothing
Residual Convergence	10^{-5}

2.6 Domain and mesh independence

Due to the steady-state treatment in the moving reference frame, a multi-zone geometry is used, consisting of a rotating disk zone containing the propeller inserted in a static cylindrical zone. The dimensions of the domain are shown in Figure 3 as a function of the propeller diameter D.

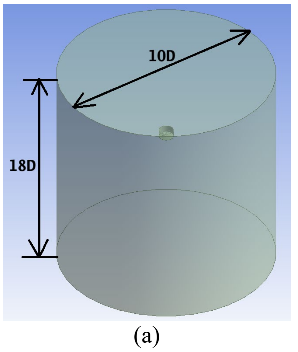

(a)

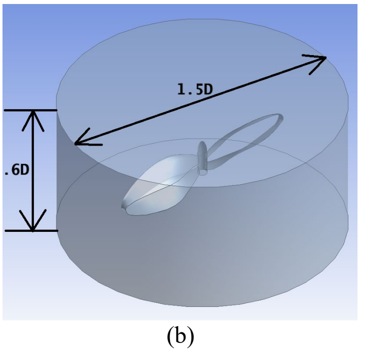

(b)

Fig. 3 – Overview of the computational domain; (a) static cylindrical zone and (b) rotating disk zone

A mesh independence study was done to determine the required resolution. A sequence of three meshes was generated using a surface refinement ratio of 2, meshes whose properties are summarised in Table 4. All meshes are unstructured, using tetrahedral (TET) cells and 5 layers of prismatic cells in the vicinity of the propeller wall, with a constant $y^+ = 50$.

Table 4 – Mesh settings used for mesh independence study

Grid	**Target TET Cell Size [mm]**	**Cell Size on Wall [mm]**	**Wall Size y^+**	**No. of Cells**
Coarse	100	2	50	1,960,000
Medium	50	1	50	3,020,000
Refined	25	0.5	50	6,290,000

The results of the mesh independence study are presented in Table 5. These show that an asymptotic rate of convergence very close to unity is obtained for all three performance coefficients. The relative error between the results obtained on the refined mesh and the Richardson extrapolation is significantly below 1% for the thrust coefficient, and slightly above 1% for torque and power coefficients.

Table 5 – Summary of mesh independence study results

	C_T	C_Q	C_P
Coarse Grid Result	0.05792	0.00975	0.06126
Medium Grid Result	0.05447	0.00948	0.05956
Refined Grid Result	0.05391	0.00935	0.05875
Richardson Extrapolation	0.05380	0.00923	0.05799
Range of Convergence	0.990	0.986	0.986
Refined Relative Error [%]	0.202	1.308	1.308

3. RESULTS AND DISCUSSIONS

3.1 Verification

To verify the accuracy of the numerical setup, a comparison is made against experimental data. The propeller selected for the comparison, the APC 12x10, has the same diameter, number of blades and blade aerofoil section as the MIL or Toroidal propeller. Information about the geometry of the propeller can be found on the manufacturer website [34]. The experimental data was retrieved from the UIUC propeller results database [35]. The propeller was tested at a constant RPM of 5019, while the airspeed was varied between 10 m/s and 23 m/s. The numerical setup uses the same solver settings as presented in Table 3, the same domain as shown in Figure 4 and the same mesh settings as found following the mesh independence study. Overall, there is an acceptable match of the experimental results. For low and medium thrust coefficient values, the torque and power coefficient predictions are excellent. For higher thrust coefficients, a small underestimation of torque and power is observed. The thrust coefficient itself is underestimated in the low-medium range of advance ratios and overestimated in the medium-high range. This behaviour of the thrust coefficient also leads to the differences observed in the propeller efficiency predictions. The differences must not be fully attributed to the numerical solver. The geometry information available on the manufacturer website [34] only includes blade data for $r/R > 0.25$, and the UIUC database [35] provides no detail on how the inner part of the blade, and the hub were designed and manufactured prior to wind tunnel testing. It is considering these differences that the match is deemed acceptable.

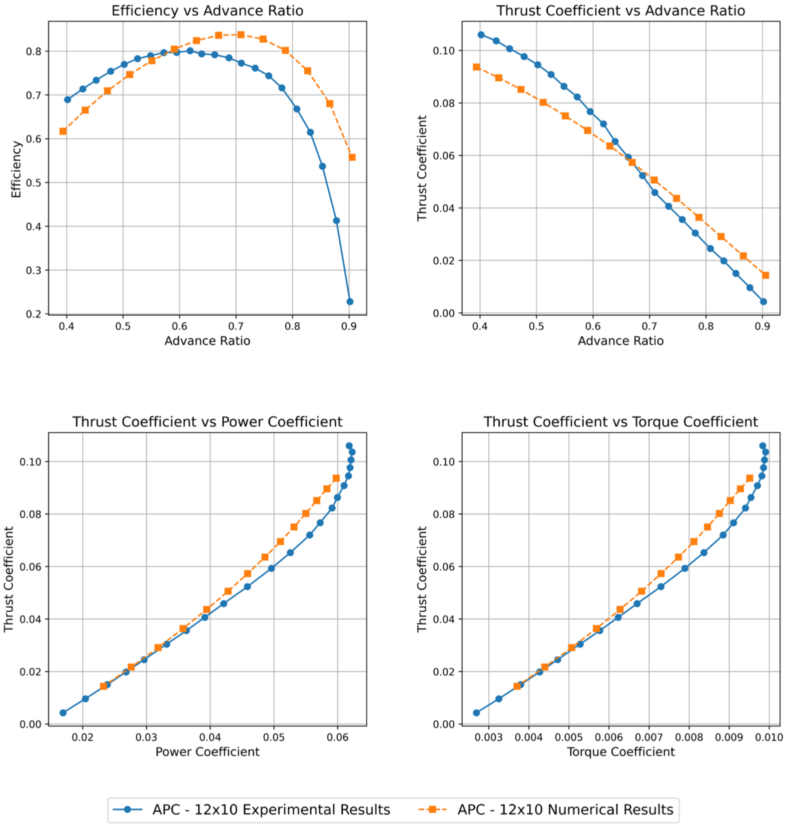

Fig. 4 – Comparison of efficiency, thrust coefficient, power coefficient and torque coefficient for the APC 12x10 propeller between experimental and numerical results

3.2 Propeller performance

Testing the performance of the Toroidal propeller designs is made at the constant airspeed of 19 m/s (as indicated in Table 1, which summarised the design operating conditions) while the RPM is varied between 3000 and 9500 to provide a wide range of off-design conditions. This results in an advance ratio range between 0.40 and 1.25, with the design advance ratio being approximately 0.75.

Figure 5 shows the results for several propeller performance metrics. In addition to the values obtained for the two Toroidal propellers, the results for the two MIL propellers are also included as a benchmark.

Both Toroidal-1 and Toroidal-2 propellers generate a significantly higher thrust coefficient than the corresponding MIL-1 and MIL-2 propellers over much of the advance ratio range under consideration. The rate at which the thrust coefficient decreases with increased advance ratio is much greater for the Toroidal designs, indicating their suitability for higher RPM thrust generation. The increased thrust coefficient generated by the Toroidal propellers is achieved via an increased power coefficient (or, equivalently, torque coefficient) over the advance ratio range. Recalling that MIL designs represent theoretical optimality in propeller design, it is not surprising that the overall efficiency of both MIL-1 and MIL-2 propellers is higher than the efficiency of the Toroidal-1 and Toroidal-2 propellers.

Nonetheless, the Toroidal designs still achieve a reasonable level of efficiency, peaking at $\eta = 0.74$ at $J = 1.25$ for Toroidal-1 and $\eta = 0.72$ at $J = 1.07$ for Toroidal-2. A consequence of the reduced efficiency of the Toroidal propellers compared to the MIL propellers is visible in the torque coefficient required to generate a fixed thrust coefficient, which is always higher for the Toroidal propellers, though a direct comparison is not always possible due to the different ranges in achieved thrust/torque coefficients. Comparing between the (1) and (2) versions of both MIL and Toroidal propellers, version (1) generates higher thrust coefficient, but with lower efficiency due to the increased power coefficient requirements, the behaviour being consistent for both MIL and Toroidal designs.

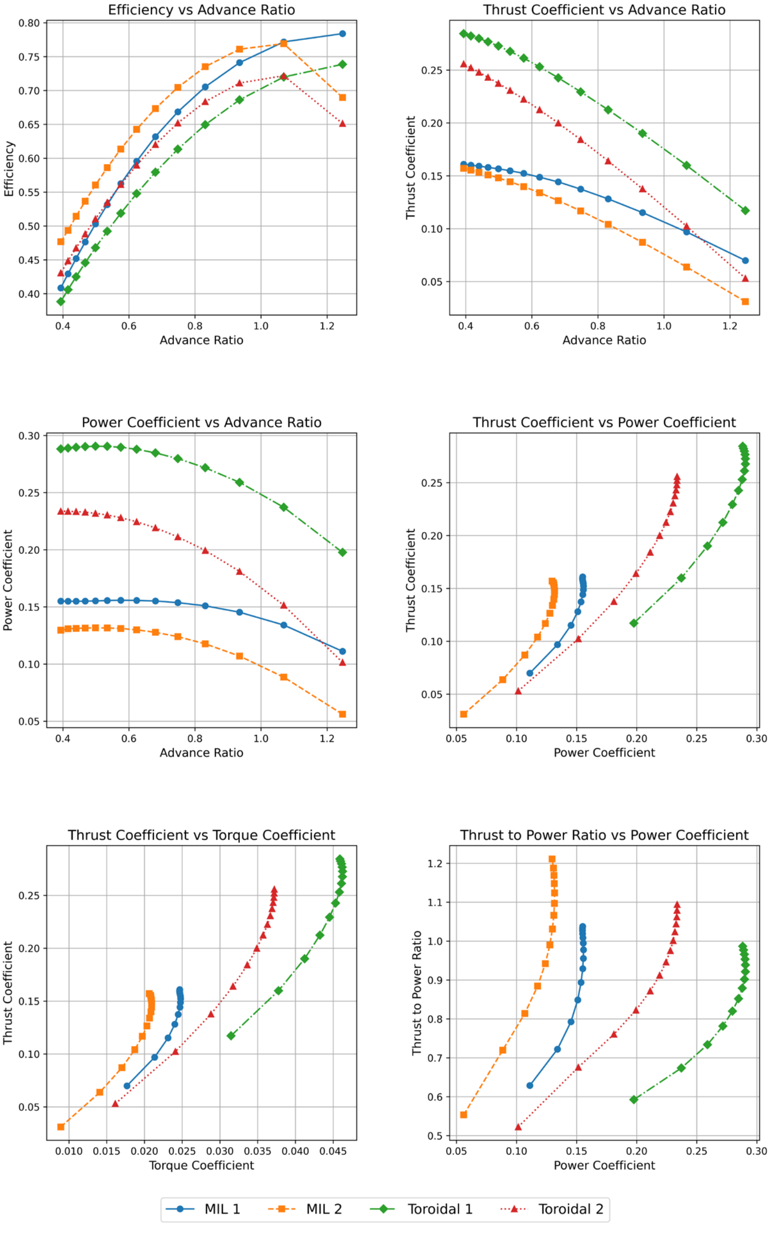

Fig. 5 – Performance characteristics of the Toroidal-1 and Toroidal-2 propellers

The performance characteristics achieved by the two Toroidal designs and depicted in Figure 5 are not typical for a 12 inch propeller aimed at low-speed electric-powered flight. To argue this point and ascertain the advantages and disadvantages of the Toroidal propellers, a set of four commercially available 2-bladed propellers of comparable diameter, pitch and operational RPM range was selected. The four propellers are the Sport 11x9, the Master Airscrew 11x10, the Aeronaut 12x13 and the APC Thin Electric 12x10. Experimental data for all four propellers are publicly available on the UIUC propeller results database [35]. Figure 6 shows the comparison between the two Toroidal propellers and the four commercially available propellers made for several performance characteristics.

Over the advance ratio range considered, the operation of both Toroidal propellers results in significantly higher thrust coefficient generation, and significantly higher power coefficient requirements. The efficiency requires a more careful investigation. First, it is noted that at the design advance ratio of 0.75, all four commercial propellers achieve an efficiency higher than the two Toroidal propellers. As the toroidal designs have not gone through an optimisation process beyond using the MIL chord and blade pitch angle distributions, there is significant scope for further improvements. Second, the two Toroidal propellers demonstrate a progressive increase in efficiency across the advance ratio range, reaching peak efficiencies comparable to the commercial propellers at the top end of the range. As having higher thrust coefficient at peak efficiency is desirable, this stands to further highlight the scope for further optimisation of the Toroidal designs.

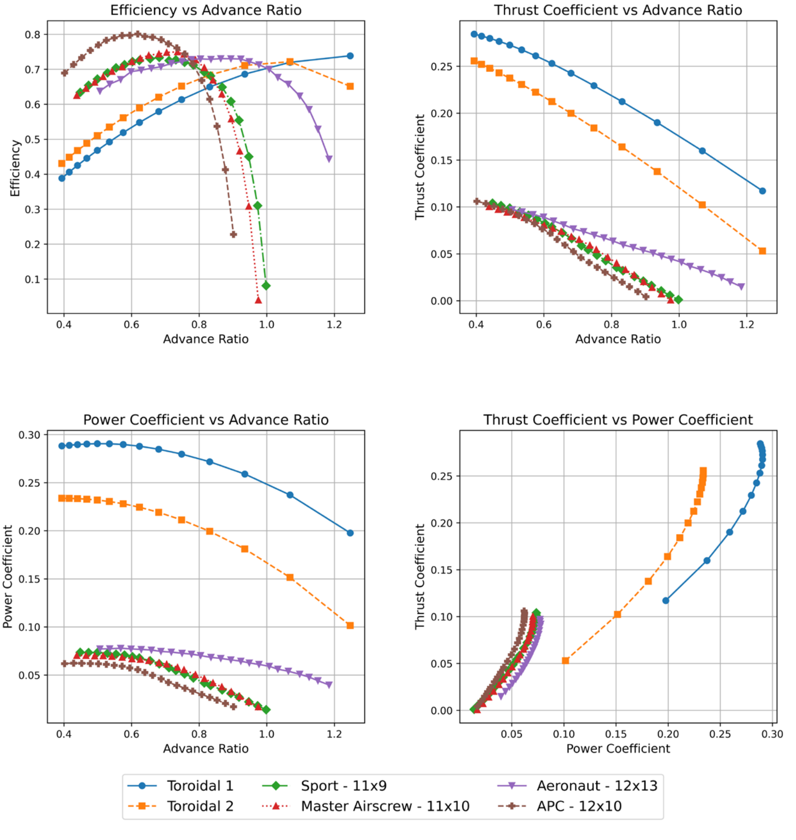

Fig. 6 – Comparison between the performance characteristics of the Toroidal-1, Toroidal-2 and four commercially available propellers

3.3 Surface flow analysis

Pressure distribution and surface streamlines can provide useful insight into the dynamics of the airflow on the propeller blades. In Figure 7, the surface pressure coefficient distribution over the propeller geometries is presented. The focus is on comparing the traditional MIL-1 and MIL-2 propellers with their respective Toroidal counterparts Toroidal-1 and Toroidal-2, while operating at the design advance ratio of $J = 0.75$. It must be noted that the pressure coefficient C_P plotted in Figure 7 is calculated using the dynamic pressure of the freestream only,

$$C_P = \frac{p_\infty - p}{\frac{1}{2}\rho_\infty V_\infty^2} \tag{6}$$

Where p_∞, ρ_∞ and V_∞ are the freestream static pressure, density and airspeed, and p is the local static pressure. The local dynamic pressure that a propeller blade sees is much higher than the freestream dynamic pressure due to the rotational velocity Ωr. By neglecting this rotational velocity in the calculation of the pressure coefficient, the resulting values will be much higher (in magnitude) compared to typical values reported in literature.

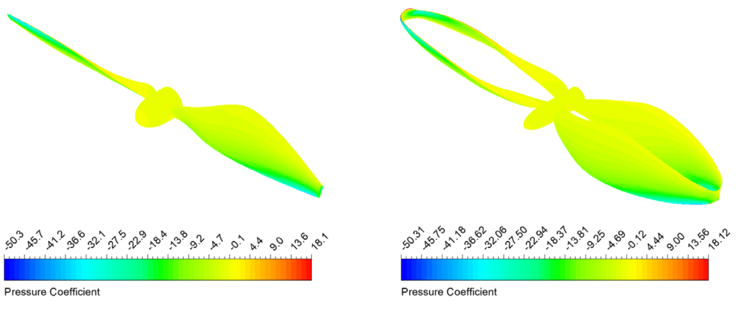

(a) MIL-1 (left) and Toroidal-1 (right)

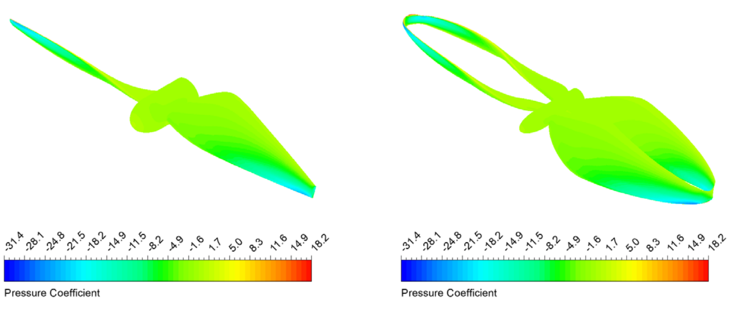

(b) MIL-2 (left) and Toroidal-2 (right)

Fig. 7 – Surface pressure coefficient distribution over MIL and Toroidal propeller geometries at an advance ratio of J=0.75

Pressure variations on both MIL-1 and MIL-2 are visibly concentrated along the blade span. The suction surfaces display significant negative pressure coefficients, indicating accelerated airflow on the blade surfaces. For MIL-1, these negative values extend down to approximately -50.3, while for MIL-2, they reach around -31.4, as shown in Figure 7. These low-pressure zones are most pronounced near the leading edges and extend mid-chord, with pressure increasing towards the trailing edges. On Toroidal-1 and Toroidal-2, the pressure distribution appears more evenly spread across their looped blade surfaces compared to the concentrated variations on MIL-1 and MIL-2. The continuous, looped shape of the Toroidal propeller blades promotes continuous airflow patterns, which can help distribute pressure more evenly.

The surface streamlines shown in Figure 8 further illustrate the differences in flow behaviour. Streamlines represent the instantaneous direction of fluid motion and provide visual representation of flow patterns. When streamlines converge, they indicate flow acceleration and a decrease in pressure. Diverging streamlines show that the flow is spreading over a larger area, causing it to slow down. If the streamlines diverge rapidly, it can potentially cause the flow to detach from the surface of the blades. Finally, parallel streamlines indicate attached flow with constant velocity and minimal pressure gradients [36].

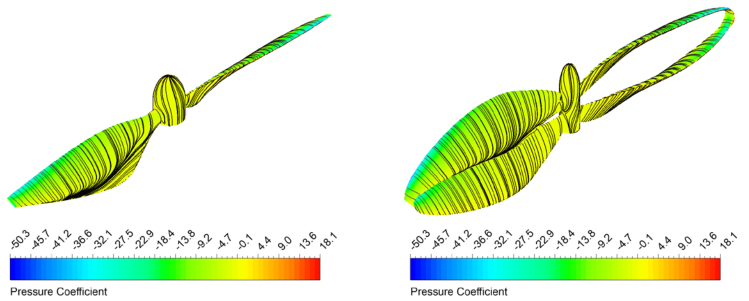

(a) MIL-1 (left) and Toroidal-1 (right)

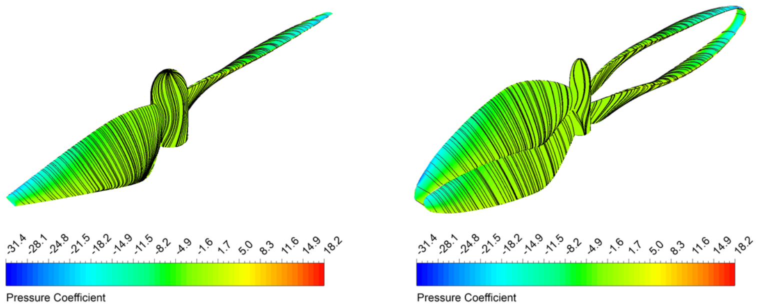

(b) MIL-2 (left) and Toroidal-2 (right)

Fig. 8 – Surface streamline visualisation over MIL and Toroidal propeller geometries at an advance ratio of J=0.75

In propellers, due to the rotation, the blade tip moves much faster than the part near the hub, causing the pressure at the tip to be even lower. This creates a pressure difference along the blade's length, pulling air outward toward the tip as it flows over the blade. When centripetal forces do not balance this radial pressure gradient, it can lead to flow separation. It can be seen from Figure 8 that on the suction sides of the MIL-1 and MIL-2 blades, the airflow converges and accelerates toward the tip, creating strong spanwise (radial) flow along the blade surface. This radial flow is much less pronounced on Toroidal-1 and Toroidal-2 blades due to their closed loop design. The design of Toroidal blades helps keep the airflow more aligned from front to back, reducing the amount of air that moves toward the tip. It should be noted that strong lateral flow can increase tip vortices, induced drag, and reduce propeller efficiency, while Toroidal designs can help mitigate these effects and improve performance [37].

3.4 Interaction between blades

Figures 9 and 10 depict static gauge pressure contours for the two Toroidal propellers in a plane perpendicular to the propeller disk plane.

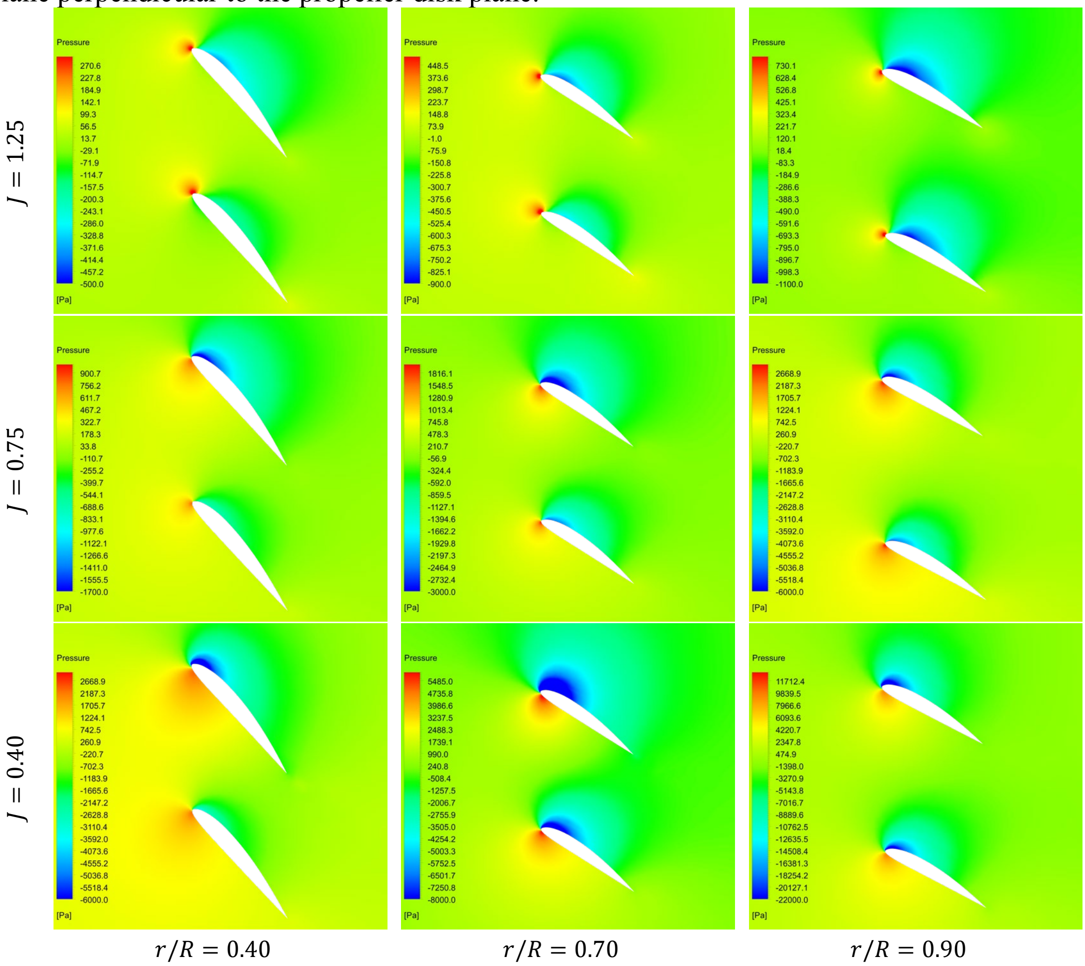

Fig. 9 – Static pressure contours at three radial positions along the blade and three advance ratio values for the Toroidal-1 propeller

Starting with the Toroidal-1 geometry (Figure 9), the pressure contour plots indicate that the spacing between the front and rear arms of the propeller is sufficient to avoid significant aerodynamic interference. Generally, the low-pressure region on the upper surface of the front arm is greater that the equivalent region on the rear arm, indicating that the front arm has a higher contribution to the thrust generation of the propeller. For the blade section located at $r/R = 0.40$, there is evidence of reduced interference across the entire range of advance angles. Moving radially outward to $r/R = 0.70$ and 0.90, the increase in the local blade velocity due to increased contribution of the rotational velocity leads to some interference between the arms, though it is limited in impact. At $r/R = 0.70$ and $J = 0.40$, the high-pressure region on the lower surface of the front arm and the low-pressure region on the upper surface of the rear arm interact, resulting in a modified pressure distribution over the aerofoil sections of both blades [18]. For $r/R = 0.90$, the interaction is even more pronounced, and it is discernible over the entire range of advance ratios. While this locally affects the thrust generation and leads to higher sectional drag (and higher contribution to propeller torque) [11,18], the specific chord distribution utilised by the propeller ensures that the outboard section of the propeller has a reduced contribution to the overall forces and moments.

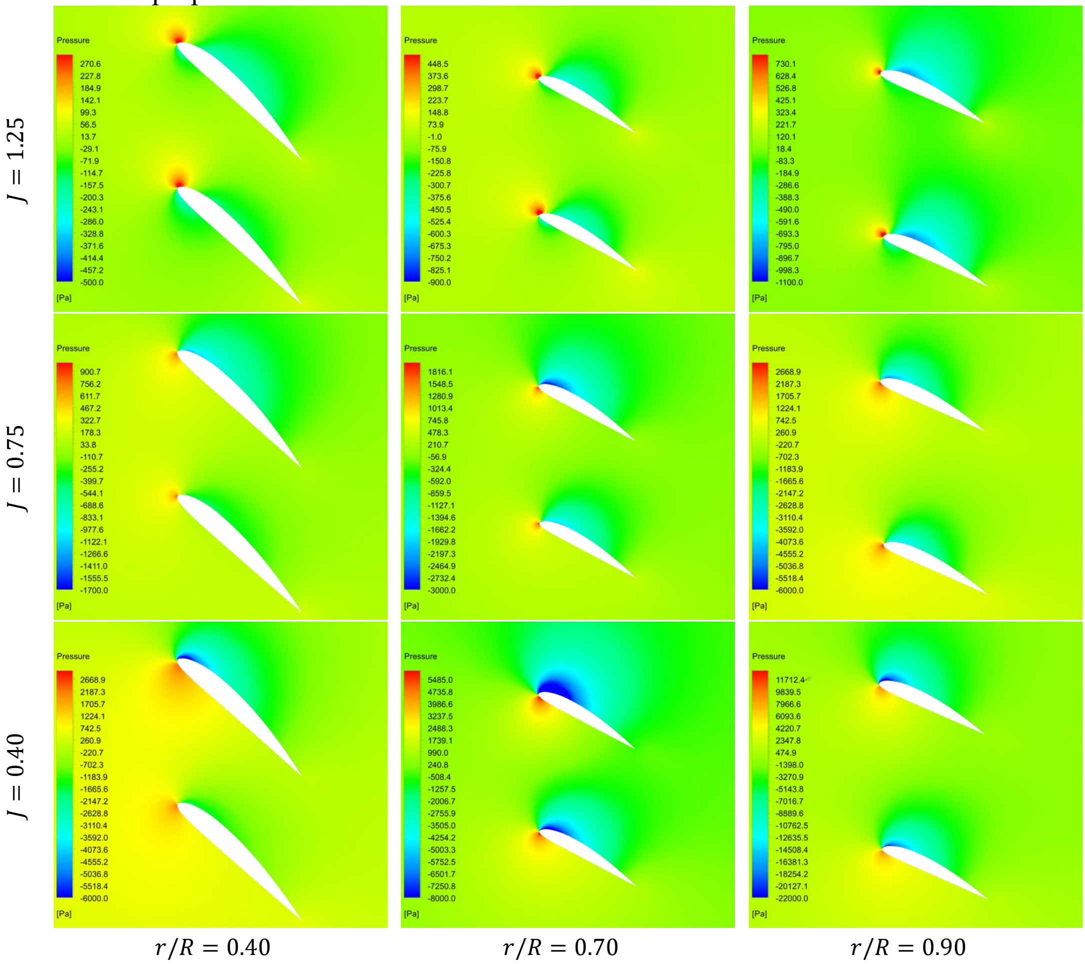

Fig. 10 – Static pressure contours at three radial positions along the blade and three advance ratio values for the Toroidal-2 propeller

For the Toroidal-2 propeller, the static gauge pressure contours depicted in Figure 10 indicate the same trends as for Toroidal-1. For $r/R = 0.40$, the interaction between the front and rear arms is limited in magnitude at all three advance ratio values, while for $r/R = 0.70$, the high-pressure region on the lower surface of the front arm and the low-pressure region on the upper surface of the rear arm interact only for $J = 0.40$. At the most outboard section of $r/R = 0.90$, the degree to which the pressure fields around the front and rear arms interact is lower that the interaction that was observed for the Toroidal-1 propeller. This is due to the blade pitch angle distribution of Toroidal-2, which uses lower pitch angle values over the entire radial span of the blade. Another consequence of the lower pitch angles is the reduced extent of the low-pressure region over the upper surface, particularly for the front arm, resulting in an overall reduction in thrust generation, but also a reduction in torque requirement.

4. CONCLUSIONS AND FURTHER WORK

This paper presented a detailed numerical investigation into the aerodynamic performance of Toroidal propellers for forward flight applications. The Toroidal propellers were designed using an in-house code and the blade chord and pitch angle distributions of two Minimum Induced Loss propellers. A steady-state Computational Fluid Dynamics analysis was conducted, incorporating multiple reference frames and the $k - \varepsilon$ turbulence model. Mesh independence was confirmed, and verification of the accuracy of the simulation model was made against experimental results by using a commercially available APC propeller. Over an advance ratio range between 0.40 and 1.25, the Toroidal propellers generate significantly higher thrust coefficients compared to the Minimum Induced Loss counterparts despite maintaining the same projected solidity, at the cost of higher torque requirements and a certain loss of efficiency. A comparison against experimental data for four commercially available propellers reveal that the Toroidal propellers can achieve comparable efficiency, but further work is required to optimise the range of advance ratios where (close to) maximum efficiency is achieved. Aerodynamic interactions between the front and rear arms of the Toroidal propeller blades can be reduced by a careful adjustment of the blade pitch angle distribution. While this reduces the thrust coefficient, it can improve the overall efficiency.

Overall, the findings support the potential of Toroidal propellers for application in a new generation of electric-powered Unmanned Aerial Vehicles. Further work should focus on local blade optimisations to maximise efficiency, aero-acoustic analysis to assess the noise characteristics and more advance turbulence modelling (e.g., Hybrid Reynolds Averaged – Large Eddy simulations) for in-depth understanding of wakes.

REFERENCES

[1] J. L. Pereira, *Hover and Wind-Tunnel Testing of Shrouded Rotors for Improved Micro Air Vehicle Design*, in Department of Aerospace Engineering, 2008, University of Maryland.

[2] W. Wei, Y. Ma, S. Wei, D. Wang, M. Guo, and Q. Yan, Analysis and Evaluation of Aerodynamic Noise Characteristics of Toroidal Propeller, *Drones*, 2024. 8(12).

[3] L. Žagar and M. Jamšek, *Comparison and Analysis of Toroidal and Classic Propellers*, in ERK'2023. 2023: Portorož.

[4] D. F. Anderson, *Understanding flight*, 2000, New York: McGraw-Hill.

[5] J. G. Leishman, *Principles of Helicopter Aerodynamics*, 2006: Cambridge University Press.

[6] C. F. Wisniewski, A. R. Byerley, and W. R. Liller, The influence of airfoil shape, tip geometry, Reynolds number and chord length on small propeller performance and noise, in *33rd AIAA Applied Aerodynamics Conference*, 2015, American Institute of Aeronautics and Astronautics.

[7] L. Stipa, *Experiments with Intubed Propellers*, 1931, National Advisory Committee for Aeronautics: Washington.

[8] W. Kruger, *On Wind Tunnel Tests and Computations Concerning the Problem of Shrouded Propellers*, 1944, National Advisory Committee for Aeronautics: Washington.

[9] S. Yilmaz, D. Erdem, and M. S. Kavsaoglu, Performance of a ducted propeller designed for UAV applications at zero angle of attack flight: An experimental study, *Aerospace Science and Technology*, 2015, 45: p. 376-386.

[10] J. Wu, Q. Wang, H. Deasy, and J. Hang, A Study on the Effect of Toroidal Propeller Parameters on Efficiency and Thrust, *Energies*, 2024, **17**(23).

[11] X.-D. Vu, A.-T. Nguyen, T.-L. Nha, H.-Q. Chu, and C.-T. Dinh, Numerical Aerodynamic and Aeroacoustic Analysis of Toroidal Propeller Designs, *International Journal of Aviation Science and Technology*, 2024(01): p. 20-33.

[12] A. Alm, W. P. Garrison, V. R. C. Gomes, C. H. Harris, G. T. Shrauger, C. Whitacre, and D. J. E. Matsson, A Study of the Efficiency of Toroidal Propeller Designs, in *The Future of Engineering Education*, 2024, American Society for Engineering Education: Oregon Convention Centre.

[13] H. P. Habib, O. N. Lima, and L. Afonso Celso de Castro, *Enhancing UAV Propulsion: Insights into Toroidal Propeller Dynamics through CFD Simulations*, Ibero-Latin American Congress on Computational Methods in Engineering (CILAMCE), 2024.

[14] D. M. Black, and C. Rohrbach, *Shrouded Propellers - A Comprehensive Performance Study*, in 5th Annual Meeting, 1968, AIAA: Pennsylvania.

[15] T. Sebastian, and C. Strem, *Toroidal Propeller*, 2020, MIT: US.

[16] K. Combey, H. Chouiyakh, K. Qaissi, M. Faqir, and O. A. Elsayed, *Aerodynamic investigation of novel toroidal joined blade tips propeller*, in Delft International Conference on Urban Air Mobility 2024, 2024: Delft, Netherlands.

[17] Y. Xiang, and W. Wang, Hydrodynamic performance evaluation of pump-jet propulsion based on the toroidal propeller, *Ocean Engineering*, 2024.

[18] C. Wang, S. Liu, K. Xia, C. Wang, and L. Ye, Numerical research on hydrodynamic performance of toroidal propeller under the influence of geometric parameters, *Ocean Engineering*, 2024.

[19] A. Ko, O. J. Ohanian, and P. Gelhausen, Ducted Fan UAV Modelling and Simulation in Preliminary Design, in *AIAA Modelling and Simulation Technologies Conference and Exhibit* 2007, American Institute of Aeronautics and Astronautics: South Carolina.

[20] R. W. Deters, G. K. Ananda, and M. S. Selig, Reynolds number effects on the performance of small-scale propellers, in *32nd AIAA Applied Aerodynamics Conference*, 2014, American Institute of Aeronautics and Astronautics: Atlanta, US.

[21] J. B. Brandt, and M. S. Selig, Propeller performance data at low Reynolds numbers, in *49th AIAA Aerospace Sciences Meeting*, 2011, AIAA Aerospace Sciences: Orlando, FL.

[22] Y. Wu, Y.-T. Ai, W. Ze, T. Jing, X. Song, and Y. Chen, A Novel Aerodynamic Noise Reduction Method Based on Improving Spanwise Blade Shape for Electric Propeller Aircraft, *International Journal of Aerospace Engineering*, 2019: p. 1-10.

[23] * * * JOUAV Unmanned Aircraft Systems, 2025, https://www.jouav.com/products/cw-007.html

[24] * * * Sparkle Tech, 2025, https://www.sparkleuav.com/drones-vtol/fixed-wing-drone/long-range-fixed-wing-uav.html

[25] * * * Athlon Avian, 2025, https://athlonavia.com/en/furia/

[26] * * * EDGE Autonomy, 2025, https://edgeautonomy.io/uncrewed-systems/penguin-c-mk2/

[27] * * * T-Motor MN3110 Multirotor Fixed Wing UAV Motor, 2025, https://store.tmotor.com/product/mn3110-motor-navigator-type.html

[28] * * * T-Motor Air 2216, 2025, https://store.tmotor.com/goods-727-Air2216T1045.html

[29] * * * XROTOR, 2025, https://web.mit.edu/drela/Public/web/xrotor/

[30] W. F. Phillips, 2004, *Mechanics of flight*, 135–145, Wiley, Hoboken, NJ, United States

[31] * * * ANSYS, 2025, https://www.ansys.com/products/fluids/ansys-fluent

[32] B. E. Launder, and D. B. Spalding, 1972, *Lectures in Mathematical Models of Turbulence*, Academic Press, London, England.

[33] S. V. Patankar, 1980, *Numerical Heat Transfer and Fluid Flow*, McGraw-Hill, Washington, New York, London.

[34] * * * Advanced Precision Composites (APC) Propellers, 2025, https://www.apcprop.com/

[35] * * * UIUC Propeller Data Site, 2025, https://m-selig.ae.illinois.edu/props/propDB.html

[36] U. Ali, E. Chadwick, and O. Sugar-Gabor, 2022, An Optimisation of a Chordwise Slot to Enhance Lateral Flow Control on a UCAV, *INCAS Bulletin*, **14**(4): p. 3-17, https://doi.org/10.13111/2066-8201.2022.14.4.1.

[37] B. W. McCormick, 1995, *Aerodynamics, Aeronautics, and Flight mechanics*, Vol. **2**. New York: Wiley.